TRIPLE RESONANCE NUCLEAR MAGNETIC RESONANCE BACKBONE ASSIGNMENT OF THE α_x I-DOMAIN INTEGRIN PROTEIN

A Senior Honors Thesis Presented to

the Faculty of the Department of Biology and Biochemistry

University of Houston

In Partial Fulfillment

of the Requirements for the Degree

Bachelor of Science

By

Omar Abousaway

May 2019

TRIPLE RESONANCE NUCLEAR MAGNETIC RESONANCE BACKBONE ASSIGNMENT OF THE αx I-DOMAIN INTEGRIN PROTEIN

_____

Omar Bassam Abousaway

APPROVED:

_____

Mehmet Sen, Ph.D.
Committee Chair

_____

Jennifer Asmussen, Ph.D.

_____

Josephine Ferreon, Ph.D.
Baylor College of Medicine

_____

Dan Wells, Ph.D.
Dean, College of Natural Sciences and Mathematics
Department of Biology and Biochemistry

To my family

ACKNOWLEDGMENTS

I would first like to thank my supervisor, Dr. Mehmet Sen. Over the years, Dr. Sen served not only as a research advisor, but a great friend. It is because of his continued belief in me despite repeated failures in the lab that I was able to complete this project.

I would next like to thank my parents, Bassam, and Houson Abousaway. I sincerely appreciate their support of my professional endeavors. The work ethic you instilled in me at a young age enabled me to complete this voluntary project in a timely manner.

I want to thank my siblings, Abraham, Roba, Zena, and Hana Abousaway. You have always been true friends of mine, even in times of difficulty. In my work, I hope to set an example to my younger siblings on how to best proceed in the world.

I would next like to thank Collins Aboagye. You were one of my best friends during my time in the Sen lab. Thank you for your invaluable contribution to the project.

Thank you to Pragya Manandhar for always being kind and encouraging.

Thank you to Mohammad Dairywala for always joking around with me about the medical school admissions process. We made a great team together in the lab.

PREFACE

This thesis project focuses on the α_x I-Domain integrin protein. This protein is the ligand binding domain of $\alpha_x\beta 2$ integrin that plays a critical role in leukocyte function.

TRIPLE RESONANCE NUCLEAR MAGNETIC RESONANCE BACKBONE ASSIGNMENT OF THE α_x I-DOMAIN INTEGRIN PROTEIN

An Abstract of Senior Honors Thesis

Presented to

the Faculty of the Department of Biology and Biochemistry

University of Houston

In Partial Fulfillment

of the Requirements for the Degree

Bachelor of Science

By

Omar Abousaway

May 2019

ABSTRACT

The I-domain of the α_x integrin subunit binds extracellular ligands, such as iC3b, a complement factor in the innate immune system. The expression of the $\alpha_x\beta2$ integrin on immune cells, such as dendritic cells, macrophages, and monocytes, suggests an in important role in the immune system. Integrin proteins are able to bind ligands when in the "open" conformation, but not and if so with limited affinity in the "closed" conformation. NMR experiments are able to probe molecular motions at the nanosecond timescale, and are thus ideal for studying the transition between the open and closed states in integrins. Here, we report the triple resonance NMR backbone assignment of the α_x I-domain integrin, as a preliminary experiment for future structural and dynamic studies.

TABLE OF CONTENTS

LIST OF TABLES

LIST OF FIGURES

ABBREVIATIONS

I – Domain	Inserted Domain
IPTG	Isopropyl-beta-D-thiogalactopyranoside
MHz	Mega Hertz
MIDAS	Metal Ion Dependent Adhesion Sire
NMR	Nuclear Magnetic Resonance
OD	Optical Density
ppm	Parts Per Million
SDS-PAGE	Sodium Dodecyl Sulfate Polyacrylamide Gel Electrophoresis

INTRODUCTION

Integrins

Integrins are a class of αβ heterodimeric transmembrane proteins involved in many roles including cell adhesion to the extracellular matrix, and cell migration. (*Hynes et al.*, 2002) In humans, there are 24 α subunits and 9 β subunits. (*Hynes et al.*, 2002) Integrins typically have large (700-900 residue) ectodomains, and short (40-70 residue) intracellular domains. Extracellular interactions of the α and β chains forms a headpiece structure, which is composed of α Inserted (I), β I-like, and β propeller domains. The calf-1, calf-2, and thigh domains of the α chain and EGF 1-4, and PSI of the β chain form the legs of the integrin. (*Hynes et al.*, 2002)

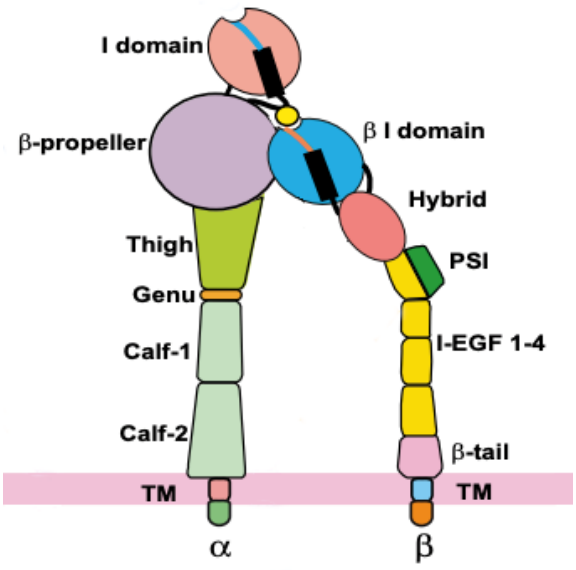

Figure 1: Integrin Domain Organization

Domain structure of the Integrin αβ heterodimer. The αI, β propeller, β I, thigh, and hybrid domains comprise the headpiece. The Integrin is shown in the extended, open conformation. Figure adapted from Chen *et al.*, 2010

Leukocyte integrins play a critical role in cell adhesion and functions in immunity. These integrins function to anchor the cell to the extracellular matrix by binding extracellular ligands, such as ICAM-1. (Aplin *et al.*, 1998) The specific ligands bound by an integrin protein varies by α-subunit composition. Activation of integrins causes leukocytes to arrest on the endothelium as a result of tight integrin binding to endothelial binding partners. (Muller, 2013)

Structural studies of integrins (mostly by electron microscopy) have revealed three overall conformational ensembles. (Figure 2) (Nishida *et al.*, 2006) In the bent form, integrins are not competent for binding. From the bent form, Integrins can undergo sweeping motions on the order of 200 Å to form the extended closed conformation. (Manadhar *et al.*, 2017) The extended closed conformation may not be capable of ligand binding. In order to enter the extended open conformation, much of the α_7 helix of the α I domain unwinds, losing helicity and the invariant Glu piston shifts down about 30 Å, allowing an allosteric relay between the α and β subunits. At the same time, the hybrid domain of the β subunit swings out from the α subunit, which allows two integrin legs to separate from each other, a signature of integrin activation. (Manadhar *et al.*, 2017; Kim *et al.*, 2003)

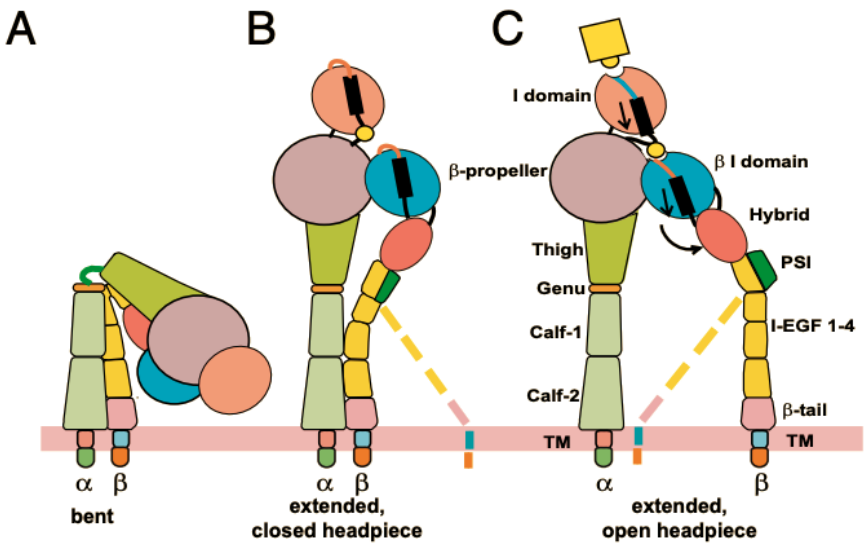

Figure 2: Three Integrin Conformations

The 3 Integrin conformations elucidated by electron microscopy. Integrins are not capable of ligand binding in the bent (**A**) and extended closed (**B**) conformation. The open, extended (**C**) conformation, characterized by a swingout of the B chain and shift of the α_7 helix is capable of ligand binding. Figure adapted from Chen *et al.*, 2010.

Integrins play a role in transmitting regulatory signals to the cell by forming focal adhesions. (Burridge *et al.*, 1996) When bound to an extracellular substrate, Integrins may bind intracellular adaptor proteins such as talin or filamin. (*Kiema et al.*, 2006) These proteins connect the integrin protein to the cytoskeleton. Intracellular signaling proteins, such as focal adhesion kinase can bind to the integrin-cytoskeleton complex and direct a cell response based signals from the extracellular matrix. (Schlaepfer *et al.*, 1994) The pathways activated the focal adhesion complex are involved in apoptosis, cell differentiation, as well as the cell cycle. (Parsons *et al.*, 2003)

The many biological roles carried out by integrin proteins have made them attractive therapeutic targets for diseases ranging from cancer to autoimmune disorders. Several Integrin-based chemotherapies are currently used in clinics and in development for treatment the of ulcerative colitis, multiple sclerosis, fibrosis, and thrombocytopenia. (Ley *et al.*, 2016)

Integrin $\alpha_X\beta 2$

The $\alpha_x\beta_2$ integrin is a member among the four β_2 integrins. (Stewart *et al.*,1995) The α_X subunit is a 127.8 kDa transmembrane protein. The ITGAX gene is located on chromosome 16 and encompasses nearly 28 kbp. The gene has 31 exons separated by 30 introns. The β2 subunit is an 84.8 kDa transmembrane protein. The ITGB2 gene is located on chromosome 21 and encompasses about 46 kbp. The gene has 16 exons separated by 15 introns.

The $\alpha_x\beta 2$ Integrin is expressed on the surface of monocytes, neutrophils, macrophages, as well as $CD8^-$ dendritic cells. (Curtis and Morrison, 2017) This integrin binds extracellular ligands including fibrinogen, iC3b, and ICAM-1. (Xu *et al.*, 2017; Frick *et al.*, 2005) iC3b is a complement protein that binds pathogens and marks them for phagocytosis. The binding of $\alpha_x\beta 2$ to iC3b is critical for phagocytosis of pathogens by immune cells. Interestingly, the binding sites of $\alpha_x\beta 2$ and $\alpha_M\beta 2$ on iC3b have no overlap. This could be advantageous and prevent immune subversion by pathogen factors. (Frick *et al.*, 2005)

Prior studies have characterized the role of $\alpha_x\beta2$ in inflammatory and antimicrobial responses. In a mouse model, knockout of $\alpha_x\beta2$ diminished recruitment of monocytes and macrophages into the peritoneum and their ability to adhere to the endothelium. (Jawhara *et al.*, 2017) This also diminished the ability of these cells to phagocytose/kill *Candida albicans* and *Escherichia coli* cells. (Jawhara *et al.*, 2017) $\alpha_x\beta2$ also appears to play a role in response to septic challenge by lipopolysaccharide. (Jawhara *et al.*, 2017)

Hence, it is clear that the $\alpha_x\beta2$ Integrin plays a role in the function of the immune system, and presents a therapeutic target for autoimmune pathologies. Structural data will be necessary for the design of agonist and antagonist compounds targeted to this protein.

α I Domains

Integrins contact the extracellular matrix through their I domains. (Lee *et al.*, 1995) Integrin I domains have a structure similar to that of G proteins, with seven α helices surrounding a β sheet core. (Figure 3) There is a coordinated magnesium ion for binding extracellular ligands within the MIDAS (metal ion dependent adhesion site) site at the "top" of the domain. (Lee *et al.*, 1995) MIDAS is formed by a DXSXS motif and present in all integrins in metazoans.

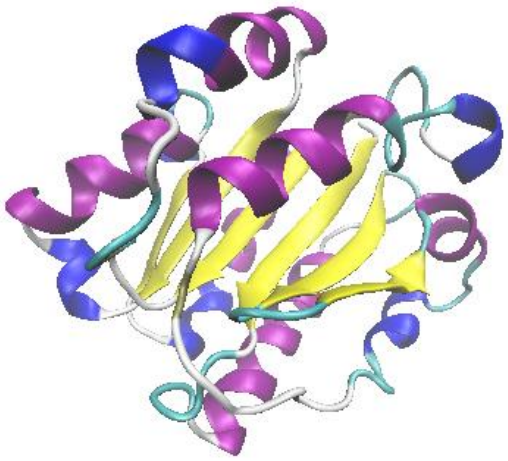

Figure 3: α_x I Domain Crystal Structure

The α_x I Domain, represented as a cartoon. Seven alpha helices surround a beta sheet core. Adapted from crystal structure PDB ID: 1N3Y

Ligand binding requires a dramatic conformational shift in the structure of the α_x I Domain. (Sen, 2013; 2016) The magnesium-binding domain reorganizes to increase exposure of the magnesium ion to the solvent. This motion results in the formation of a negative potential around the positively charged magnesium ion. (Shimaoka et al., 2003) This motion is also coupled to a unwinding of much of the α_7 helix and a 30 Å downward shift of the invariant Glu piston, allowing allosteric relay between the α and β subunits. (Takagi and Springer, 2002)

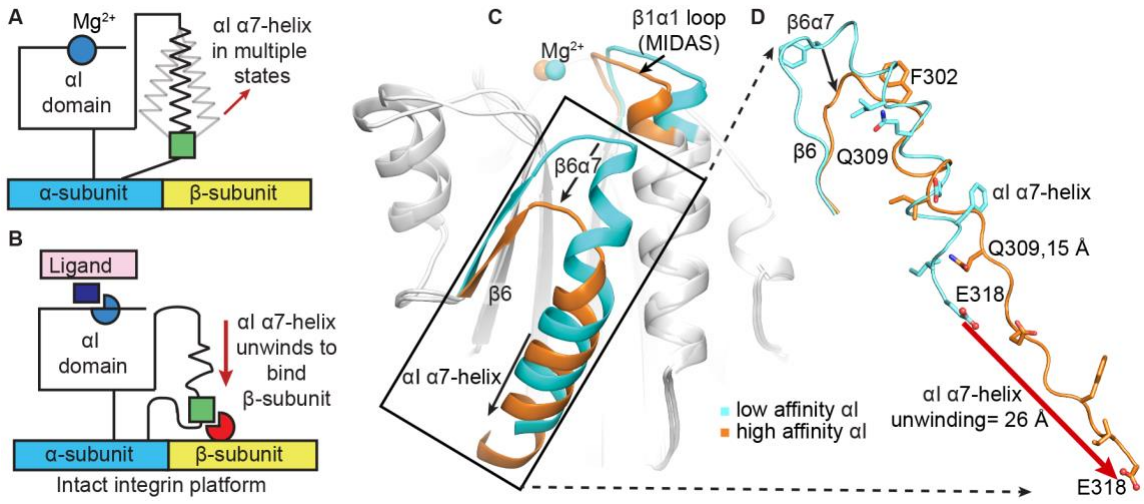

Figure 4: Current Model of α_7 Helix Motions in Integrin Activation

A and **B** show the current model, in which ligand binding induces a downward shift in the α_7 helix. **C** and **D** show conflicting structures for the activated αI domain. **C** shows overall conformational shifts that take place in the I domain upon activation. **D** the unwinding of the α_7 helix. Adapted from Manandhar et al., 2017.

The molecular motions inherent to I domains must be understood prior to drug development efforts targeted at these proteins.

Nuclear Magnetic Resonance

Previous studies have published several X-ray crystal structures of the α_x I Domain. These include a structure of the α_x I domain alone, and an ectodomain structure of $\alpha_x\beta 2$ in the closed and metastable states. (Vorup-Jensen *et al.*, 2003; Sen, 2013 and 2016) These structures are collected by diffraction data, and represent average positions of atoms in the closed state. These crystal structures do not provide data describing the molecular motions of the α_x I domain in its transition between the closed and open forms.

In fact, there are currently no crystal structures describing the open form of the α_x I domain.

Nuclear magnetic resonance spectroscopy is a widely used technique for the study of molecular structure. Molecules, such as proteins, in solution are exposed to a strong static magnetic field perturbed by a weak oscillating magnetic field. This is used to determine the chemical shifts of atoms in the sample, which can be used for studying the structure of the molecule in solution.

One of the most common experiments in protein Nuclear Magnetic Resonance Spectroscopy is ^{15}N heteronuclear single quantum coherence (HSQC). This experiment measures the chemical shift of the amide nitrogen and amide hydrogen. The output of this experiment is a spectra plotting the chemical shift the nitrogen against the hydrogen. Each amino acid in a protein has distinct chemical shift values and hence corresponds to unique peak in the HSQC. HSQC experiments can be conducted on a protein under varying concentrations of a small molecule to identify interacting residues. Thus, the HSQC experiment is a valuable source of data for the purpose of drug design. (Cavanagh *et al.*, 2007)

The process of identifying or assigning the peaks in the HSQC spectra that correspond to each amino acid in a protein is called an NMR backbone assignment. This process relies on the use of triple-resonance experiments such as HNCA and HNCACB to correlate

HSQC peaks to amino acids in a protein. The NMR backbone assignment of a protein is an important preliminary project undertaken prior to NMR structural studies.

Because of the molecular motions inherent in Integrin I domains, and X-ray crystallography's inability to probe these motions, NMR studies of the α_x I domain are necessary to understand the structural dynamics of the protein in solution. As there have been no prior NMR studies of the α_x I domain, an NMR backbone assignment must be undertaken prior to future NMR studies of this protein.

Specific Aims

The goal of this project is to complete an NMR backbone assignment of the α_x I domain. This project will allow for future NMR studies that seek to understand the molecular motions of the α_x I domain in solution in the presence and absence of small molecule drugs and cations.

METHODS

Expression and Purification of α_x I domain

DNA for the α_x I domain were cloned into the pet28a expression vector. This plasmid was then transformed into *E. coli* expression BL21 Rosetta cells and tested for overexpression of the protein. Inoculated cells were grown until they reached 0.6 OD_{600} and resuspended in 5 mL LB media at 37 °C. Expression was then induced by 1 mM isopropyl-β-D-thiogalactopyranoside (IPTG). Following overnight expression, 1 mL of cells were centrifuged at 13,000 rpm, and tested for expression by SDS-PAGE gel analysis. The gel was stained with Coomassie Brilliant blue G-250 and destained to observe protein expression.

Expression of Triple-labelled α_x I domain in Minimal Media

To produce $^{13}C/^{15}N/^{2}D$ -labelled α_x I domain for further NMR experimentation, the expression construct was transformed into BL21 Rosetta E. coli cells. These cells were used to inoculate a 5 mL LB for overnight growth in the presence of kanamycin and chloramphenicol at 37 °C with orbital shaking at 250 rpm. 1 mL of prepared minimal media containing $(N^{15}H_4)_2SO4$ and $N^{15}H_4Cl$ as the only nitrogen sources, filter sterilized D_2O, and C^{13}-labelled D-Glucose as the only carbon source was added to 3.5 mL LB media. The components of the minimal media are listed in the appendix. 0.5 mL of the starting culture was added to this media and allowed to grow overnight. 2 mL of this

overnight culture was added to 5 mL D_2O containing minimal media and allowed to grow until it reached an OD_{600} of 1.5. This culture was then centrifuged for 25 min at 4,000 rpm. The supernatant was discarded and the pellet was resolubilized in 100 mL of D_2O containing minimal media. This culture was then allowed to grow overnight at 37 °C until it reached a OD_{600} of 2.5. This overnight culture was added to 1L of D_2O containing minimal media and allowed to grow until the OD_{600} reached 0.9. Expression was then induced by addition of 1 mM IPTG. After overnight growth at 27 °C, cells were harvested by centrifugation at 6,000 rpm. The supernatant was placed in the orbital shaker for 48 hrs to allow regrowth of any unpelleted cells. This was then recentrifuged and cells were harvested. Expression was assessed by SDS PAGE gel electrophoresis.

Expression of Double-labelled α_x I Domain in Minimal Media

To produce uniformly $^{15}N/^{13}C$-labelled α_x I domain for NMR experiments, the expression construct was transformed into BL21 RIL strain of *E. coli*. These cells were used to inoculate a 5mL LB for overnight growth in the presence of Kanamycin and chloramphenicol at 37 °C with orbital shaking at 250 rpm. 500 µL of this overnight culture was used to inoculate a 500 mL minimal medial containing $(N^{15}H_4)_2SO4$ and $N^{15}H_4Cl$ as the only nitrogen sources. Components of the minimal media are listed in the appendix. When the bacterial culture reached OD_{600}, expression was induced by adding 1 mM IPTG. After overnight growth, cells were harvested by centrifugation at 6,000 rpm. Expression was assessed by SDS PAGE gel electrophoresis.

Purification

Purification of N^{15}-labelled and triple-labelled samples was carried out separately but followed the same protocol. Harvested cells containing the Histaged protein were lysed by homogenization in 8.0 pH 20 mM tris, 200 mM NaCl. 2X PMSF and 1000X were added to the cell lysate. Cell lysate was then left to shake at 4 °C for 1 hour. Cell lysates were centrifuged at 10,000 rpm at 4 °C for 5 mins and the insoluble pellet was discarded. The soluble cell lysates were then loaded onto a 10 mL Ni-NTA column for purification by affinity chromatography. After loading the cell lysate, a buffer consisting of 20 mM tris, pH 8.0, 300 mM NaCl, 10% glycerol, 40 mM imidazole was passed through the column at a rate of 2 mL/min. A linear gradient of a buffer consisting of 20 mM tris, pH 8.0, 300 mM NaCl, 10% glycerol, 500 mM imidazole was used to elute the protein from the column. Fractions were assessed by SDS-PAGE to check which fractions contained the protein. Fractions containing the α_X I Domain were pooled to a final volume of 4.0 mL. After equilibrating a size exclusion column with running buffer (50 mM MES, pH 6.0, 10 mM $MgCl_2$, 10 mM glutamate), the α_X I Domain was purified by size exclusion and fractions were analyzed for expression by SDS-PAGE. Fractions containing α_X I Domain were pooled.

NMR Sample Conditions

Isotopically labelled samples in the size exclusion buffer were concentrated to a final concentration of 10 mg/mL and buffer exchanged to an NMR buffer (50 mM MES, pH 6.0, 10 mM $MgCl_2$, 20% D_2O, .04% NaN_3, 2X PMSF). The final volume of the NMR sample was 450 μL.

NMR Acquisition

NMR experiments were conducted on a Bruker 800 MHz equipped with a triple resonance $^{1}H/^{13}C/^{15}N$ optimized for proton detection at 293 K. Data was processed and analyzed using SPARKY software version 3.115 (Johnson 2004; Lee *et al.*, 2015). All experiments were conducted at the KECK Institute for molecular design facility at the University of Houston.

	Parameter	Value		Parameter	Value
HNCACB/CBCA(CO)NH	time domain (t1)	50	HNCA	time domain (t1)	120
	time domain (t2)	64		time domain (t2)	64
	time domain (t3)	2,048		time domain (t3)	4,096
	Spectral width (t1) Hz	11,682		Spectral width (t1) Hz	5,232
	Spectral width (t2) Hz	2,343		Spectral width (t2) Hz	2,594
	Spectral width (t3) Hz	9,615		Spectral width (t3) Hz	10,416
	Number of scans	32		Number of scans	32
	sample	^{2}H / ^{13}C / ^{15}N labeled		sample	^{13}C / ^{15}N labeled
	field strength	800 MHz cryogenic TCI probe		field strength	800 MHz cryogenic TCI probe
HN(CA)CO	time domain (t1)	90	HN(CO)CA	time domain (t1)	128
	time domain (t2)	64		time domain (t2)	60
	time domain (t3)	2,048		time domain (t3)	2,048
	Spectral width (t1) Hz	2,817		Spectral width (t1) Hz	2,414
	Spectral width (t2) Hz	2,432		Spectral width (t2) Hz	2,594
	Spectral width (t3) Hz	10,000		Spectral width (t3) Hz	11,160
	Number of scans	48		Number of scans	40
	sample	^{2}H / ^{13}C / ^{15}N labeled		sample	^{2}H / ^{13}C / ^{15}N labeled
	field strength	800 MHz cryogenic TCI probe		field strength	800 MHz cryogenic TCI probe
HNCO	time domain (t1)	90			
	time domain (t2)	64			
	time domain (t3)	1,048			
	Spectral width (t1) Hz	2,817			
	Spectral width (t2) Hz	2,432			
	Spectral width (t3) Hz	9,615			
	Number of scans	16			
	sample	^{2}H / ^{13}C / ^{15}N labeled			
	field strength	800 MHz cryogenic TCI probe			

Table I: NMR Acquisition Parameters

Triple Resonance Experiments and Backbone Specific NMR Assignment

Sequential Backbone Resonance Assignments were carried out using $^{13}C/^{15}N$ and $^{2}D/^{13}C/^{15}N$ labeled samples of the α_x I domain. 90% of assignments were obtained by through-bond triple resonance experiments including HNCACB CBCA(CO)NH, HNCO, HNCACO, NHCA, HNCOCA conducted on a Bruker 800 MHz spectrometer.

RESULTS

The α_x I domain was cloned into the pet28a expression vector. The expressed protein was first purified by affinity chromatography using a Ni NTA agarose column. The protein was eluted from the column by gradually increasing the concentration of imidazole. The protein was then further purified by size exclusion chromatography. SDS PAGE was then used to confirm the presence of the protein. This process was the same for both $^{13}C/^{15}N$ and $^{2}D/^{13}C/^{15}N$ labeled samples of the protein. Purification of the $^{13}C/^{15}N$ labeled protein is presented in figure 5. Ni NTA purification is demonstrates in 5A, Size Exclusion in 5B, and the SDS PAGE gel in 5C. Purification of the $^{2}D/^{13}C/^{15}N$ labeled protein is presented in figure 6. Ni NTA purification is demonstrates in 6A, Size Exclusion in 6B, and the SDS PAGE gel in 6C.

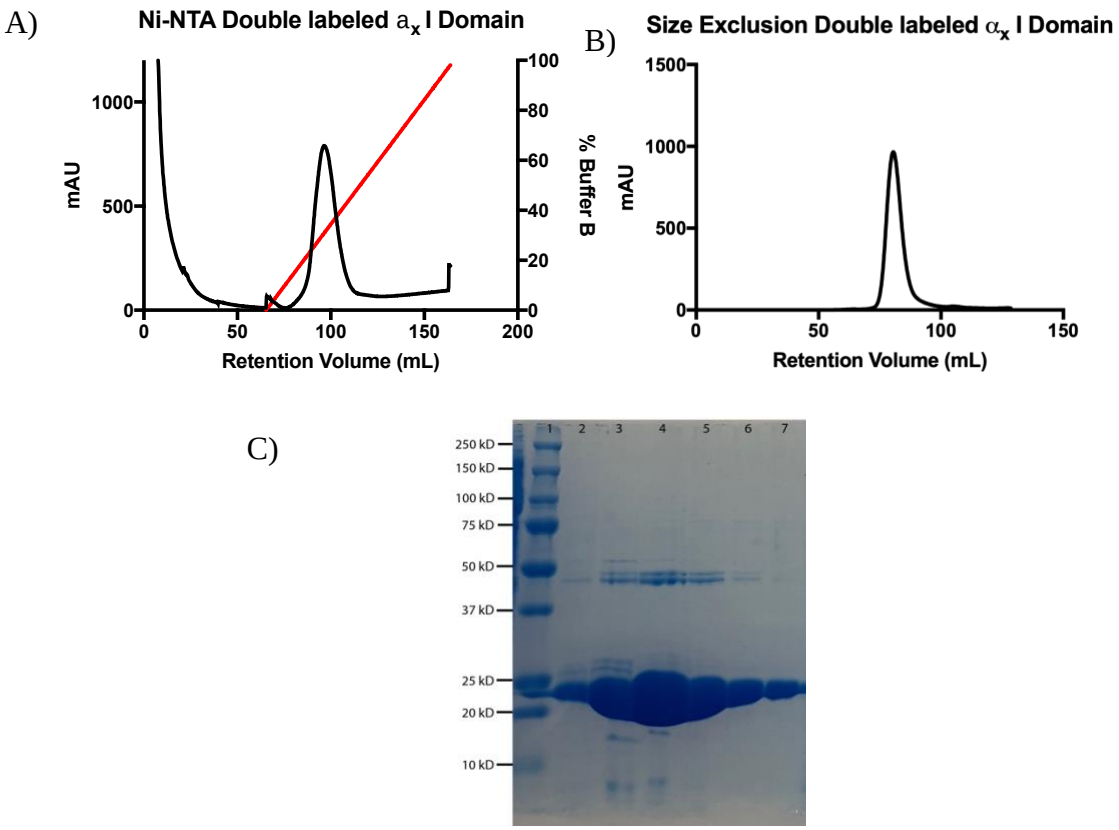

Figure 5: Purification of Double Labeled αX I Domain

A) Affinity chromatography purification of double labeled α_x I domain using a Histrap 10 mL column. Protein was eluted by increasing the concentration of Buffer B relative to Buffer A by a linear gradient. Buffer A is 20 mM Tris, pH 8.0, 300 mM NaCl, 10% glycerol, and 40 mM Imidazole. Buffer B is 20 mM Tris, pH 8.0, 300 mM NaCl, 10% glycerol, and 500 mM Imidazole. **B)** Size Exclusion Chromatography (Superdex 75 Hiload 16/60) of double labeled α_x I domain. The elution time is 80 mL. Both purification steps were performed at 4 °C, with flow rates of 1 mL/min and 2 mL/min respectively. **C)** SDS-PAGE gel of purified C^{13}/N^{15} labelled α_x I domain in 12% polyacrylamide. The molecular weight standards are shown in lane 1, and labelled at the side of the gel. Fractions from size exclusion chromatography containing purified α_x I domain are shown in lanes 2-7. The bands at 20 kD correspond to the α_X I domain.

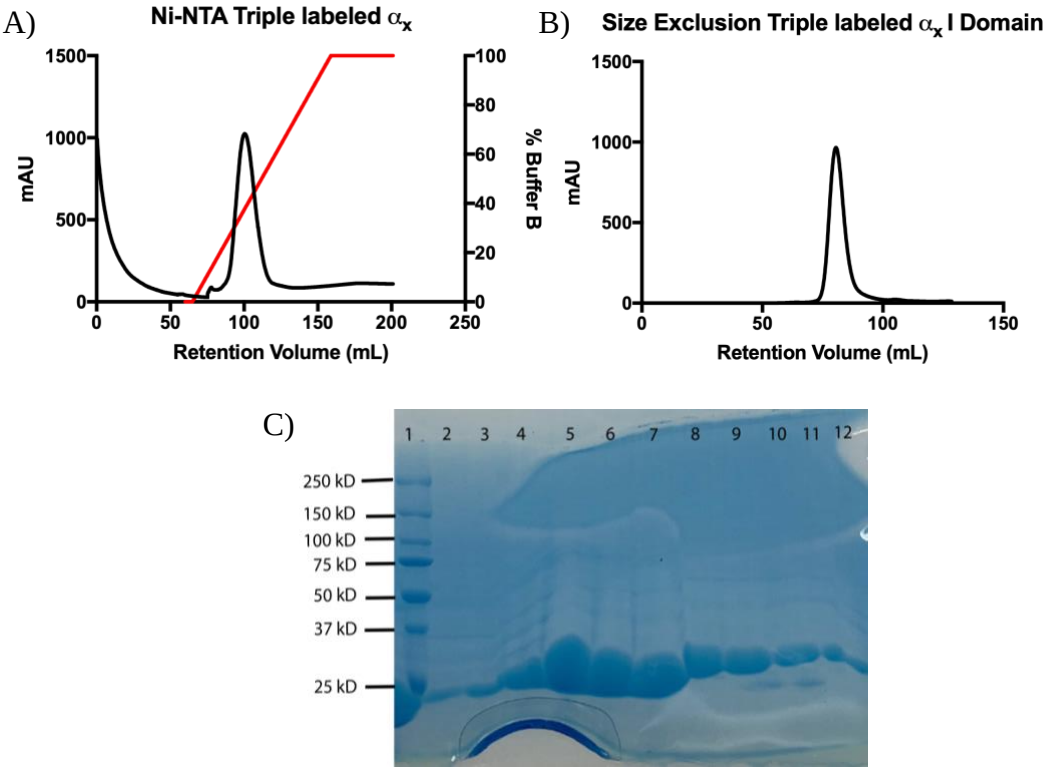

Figure 6: Purification of Triple Labeled α_x I Domain

A) Affinity chromatography purification of triple labeled α_x I domain using a Histrap 10mL column. Protein was eluted by increasing the concentration of Buffer B relative to Buffer A by a linear gradient. Buffer A is 20 mM Tris, pH 8.0, 300 mM NaCl, 10% glycerol, and 40 mM Imidazole. Buffer B is 20 mM Tris, pH 8.0, 300 mM NaCl, 10% glycerol, and 500 mM Imidazole. **B)** Size Exclusion Chromatography (Superdex 75 Hiload 16/60) of double labeled α_x I domain. The elution time is 100 mL. Both purification steps were performed at 4 °C, with flow rates of 1mL/min and 2 mL/min respectively. **C)** SDS-PAGE gel of purified C^{13}/N^{15} labelled α_x I domain in 12% polyacrylamide. The molecular weight standards are shown in lane 1, and labelled at the side of the gel. Fractions from size exclusion chromatography containing purified α_x I domain are shown in lanes 2-12. The bands at 20 kD correspond to the α_X I domain.

NMR backbone assignment

Analysis of HNCACB and CBCA(CO)NH experiments provided the most direct way of obtaining a sequence specific backbone assignment. Strip plots showing HNCACB and CBCA(CO)NH spectra for residues K280- D284 are shown in Figure 7.

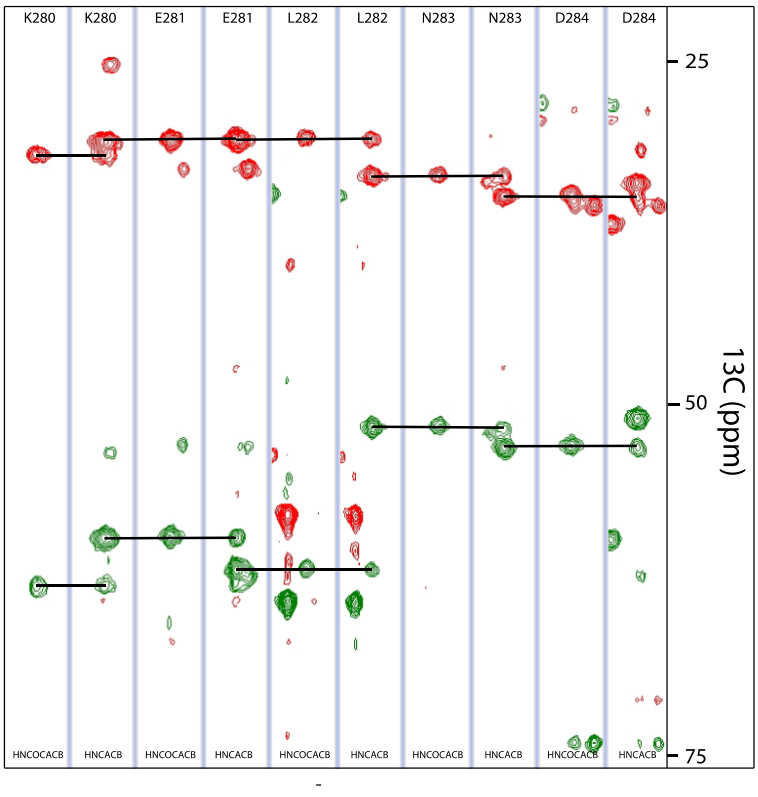

Figure 7: HNCOCACB and HNCACB Strip Plots of Residues K280-D284

Strip plots from HNCOCACB and HNCACB spectra acquired at 298 K with 5 mg/mL $^{2}D/^{13}C/^{15}N$-labeled α_x I-domain in 10% D_2O illustrating the sequential through bond connectivities of $^{13}C\alpha$ and $^{13}C\beta$. The HNCOCACB spectra at the left correlates the amide ^{1}H and ^{15}N resonance of the *i*th residue to the $^{13}C\alpha$ and $^{13}C\beta$ of the *i-1* residue. The HNCACB spectra at the right correlates the ^{1}H and ^{15}N resonance of the *i*th residue to the $^{13}C\alpha$ and $^{13}C\beta$ of the *i*th and *i-1* residue.

Carbonyl carbon chemical shift assignments were made using HNCO and HNCACO experiments. These experiments also served to corroborate and build on assignments made using the HNCACB and CBCA(CO)NH spectra. Shown in Figure 8 are strip plots of HNCO and HNCACO spectra for residues K280-D284.

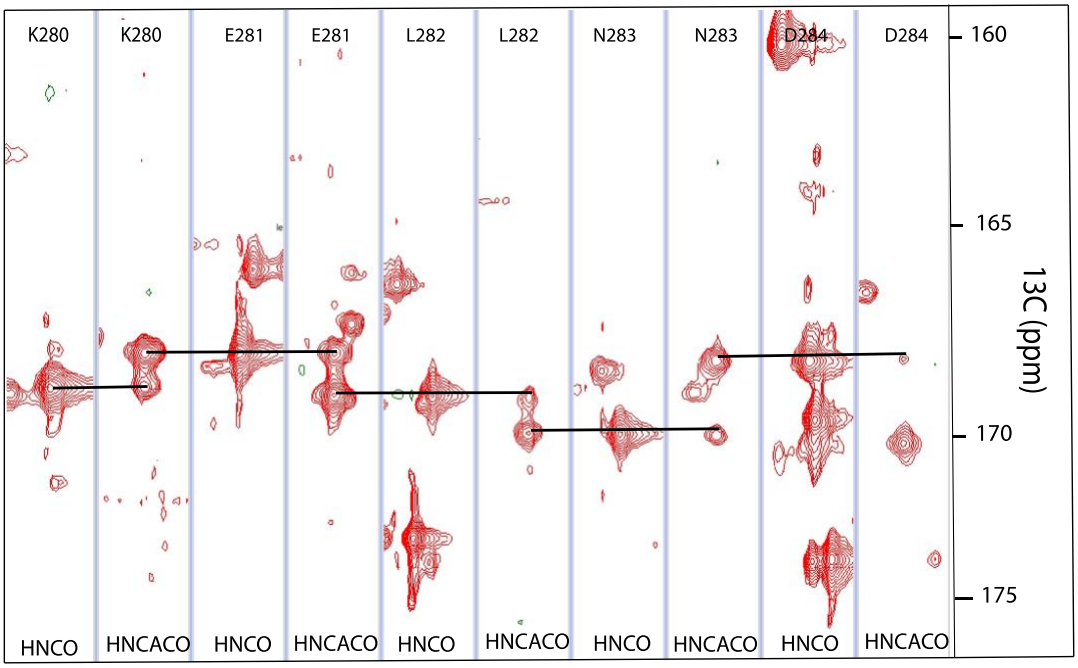

Figure 8: HNCO and HNCACO Strip Plots of Residues K280-D284

Strip plots from HNCO and HNCACO spectra acquired at 298 K with 5 mg/mL $^{2}D/^{13}C/^{15}N$-labeled α_x I-domain in 10% D_2O illustrating the sequential through bond connectivities of ^{13}CO. The HNCO spectra at the left correlates the amide ^{1}H and ^{15}N resonance of the *i*th residue to the carbonyl ^{13}CO of the *i-1* residue. The HNCACO spectra at the right correlates the ^{1}H and ^{15}N resonance of the *i*th residue to the carbonyl ^{13}CO of the *i*th and *i-1* residue.

Identification of Asn and Gln side chain amides is useful for assigning Cβ and Cα chemical resonances by an analogous manner. In the HNCACB experiment, magnetization transfer of Asn amide side chain protons to the neighboring carbons will provide the chemical shifts of the Cα and Cβ. In the same manner, magnetic transfer of the Gln amide side chain proton provides the chemical shifts of Cγ and Cβ. Analysis of these peaks provides a convenient method to confirm the Cα and Cβ assignments using the HNCACB and HNCOCACB spectra.

Identification of Glycine Cα in HNCACB and HNCOCACB spectra provided a convenient method for starting Cα and Cβ resonance assignments. In the HNCACB spectrum, glycine shows a single, distinctive (45 ppm) Cα peak and no Cβ peak. This characteristic signature, along with glycine's scarcity in the protein sequence allows for straightforward assignment of glycine and identified neighboring peaks.

Overall, 88.7% of peaks were assigned in the HSQC. Assigned amino acids are presented in Figure 9. Missing peaks included: M129, E130, V134, F135, I137, S142, V155, V159, T167, F169, S191, K233, I234, I238, T239, D240, K242, R276, S290, and I317. List of chemical shifts for assigned residues in appendix.

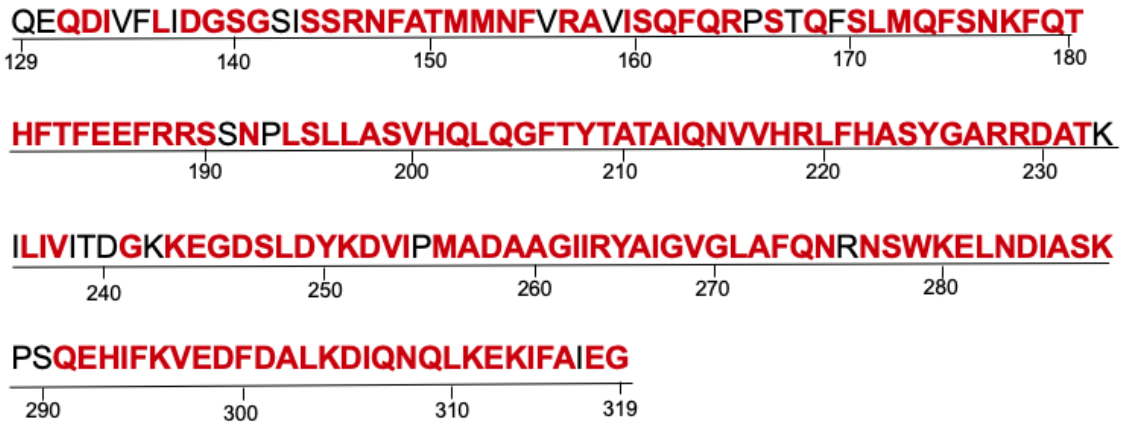

Figure 9: α_x I domain Residues Assigned in HSQC

Residues of α_x I domain assigned in HSQC spectra. Assigned residues colored in red. Residues not assigned in black.

HSQC

HSQC experiments were conducted for both $^{2}D/^{13}C/^{15}N$ and $^{13}C/^{15}N$ labelled samples. As expected, the $^{2}D/^{13}C/^{15}N$ sample showed sharper peaks in the HSQC as a result of slower tumbling caused by larger protein mass. The HSQC for the $^{13}C/^{15}N$ labeled sample is presented in Figure 10. The HSQC for the $^{2}D/^{13}C/^{15}N$ labeled sample is presented in Figure 11.

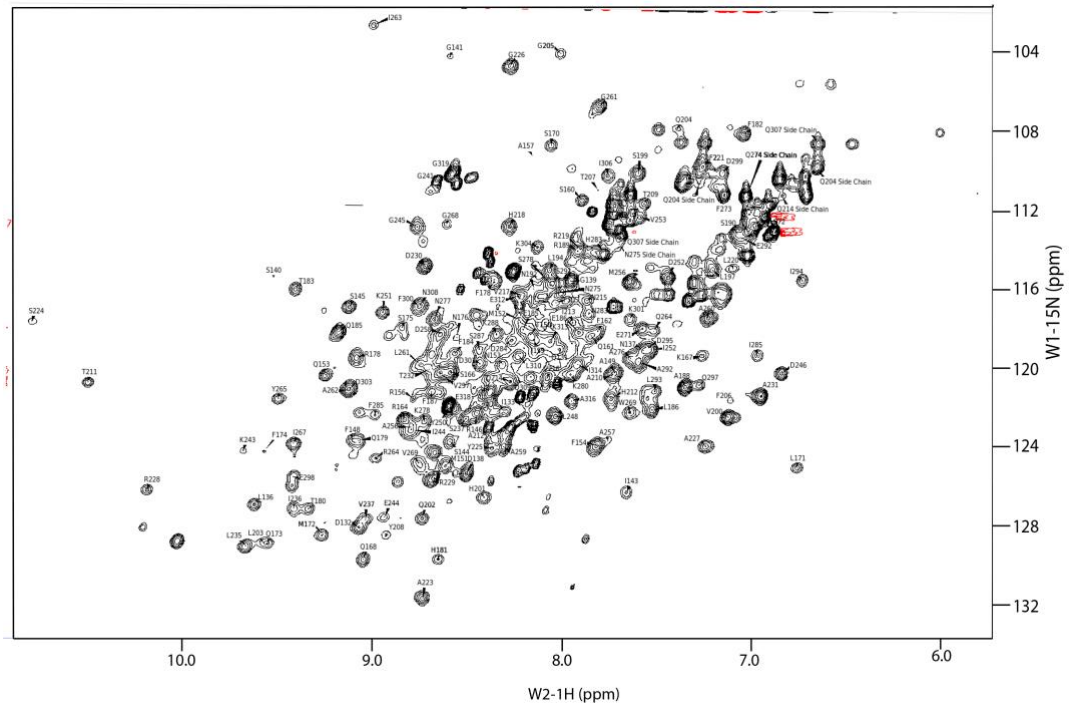

Figure 10: HSQC of Double Labeled α_x I Domain

$^{1}H/^{15}N$ HSQC of 5 mg/mL $^{13}C/^{15}N$-labeled α_x I-domain with an N-terminal hexameric Histidine Tag in 25 mM MES (pH 7.0) with 128 scans acquired on 800 MHz Bruker Spectrometer.

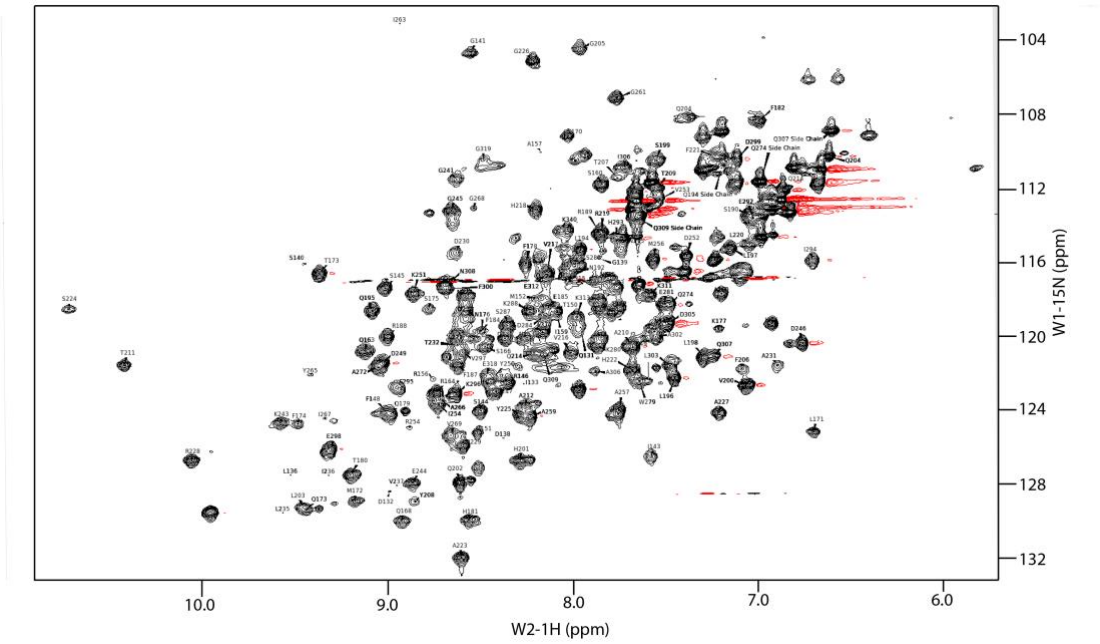

Figure 11: HSQC of Triple Labeled α_x I Domain

$^{1}H/^{15}N$ HSQC of 5mg/mL $^{2}D/^{13}C/^{15}N$-labeled α_x I-domain with an N-terminal hexameric Histidine Tag in 25 mM MES (pH 7.0) with 128 scans acquired on 800 MHz Bruker Spectrometer.

The HSQC spectra obtained for the $^{2}D/^{13}C/^{15}N$-labeled sample has an excellent dispersion of peaks relative to the HSQC of the $^{13}C/^{15}N$-labeled sample. Hence, the HSQC of the $^{2}D/^{13}C/^{15}N$-labeled sample served as the template for most of the backbone assignment. However, the HSQC of the $^{13}C/^{15}N$-labeled sample provided resonances for residues not observable in the HSQC of the triple-labelled sample, such as I263.

Interestingly, in both the double and triple-labelled HSQC, there are several sets of 'leak out' peaks neighboring principal peaks, which show identical resonances in triple-resonance experiments. Leak out peaks are present in residues 149-152 and 296-306. These leak out peaks could point to ensembles of alternate conformations the protein

occupies in solution. In each alternate conformation, the local environment of an amino acid differs, resulting in changes to chemical shift values.

DISCUSSION

As a result of this study, 88.7% of the assignable residues of the α_x I domain (which does not include proline) were assigned in the HSQC spectra. This is the first extensive NMR assignment obtained for this protein. This data will allow NMR studies probing the motions of the α_x I domain at the nanosecond timescale. Such studies can elucidate how the protein behaves in solution and either validate or disprove the current model of α_x I domain activation. Of particular interest would be probing the motions of the α_7 helix, which is thought to be highly flexible in the closed conformation. What could also be elucidated is the structural mechanism of the transition between the open and closed conformations.

HSQC spectra obtained for both the $^{2}H/^{13}C/^{15}N$ and $^{13}C/^{15}N$ labeled protein were invaluable to the assignment. As expected, the HSQC spectra for the $^{2}H/^{13}C/^{15}N$ labeled I domain had sharper peaks than the $^{15}N/^{13}C$ labeled sample. As a consequence, the HSQC for the $^{2}H/^{13}C/^{15}N$ labeled sample was a more suitable template for much of the assignment. However, referring to the HSQC for the $^{13}C/^{15}N$ labeled sample allowed for the assignment of residues for which peaks were not found in the HSQC for the $^{15}N/^{13}C/^{2}H$ labeled sample. This is particularly true for many N-terminal residues, for which much data was lacking in the HSQC for the $^{2}H/^{13}C/^{15}N$ labeled sample. It is not clear why certain peaks were only present in the HSQC for the double labeled sample.

An important and unexpected finding is the appearance of leak out peaks in residues in 149-152 and 296-306. The presence of these peaks suggests that the protein exists in more than one ensemble of conformations in solution. This is the first report of this finding. The residues A149-M152 are found in the α1 helix, and residues 296-306 compose the β6-α7 loop. These are the residues that are most affected by the suggested transition between alternate conformational states. Given that the β6-α7 loop has been found to move in the transition between the open and closed conformational states, this data might suggest that the α_x I domain in both the open conformation and closed conformations in solution. This could be significantly biologically relevant, because it suggests that the α_x I domain can exist in the ligand binding-competent state without the need of an intracellular signal.

This data can also aid future drug development efforts. The chemical shifts obtained represent the α_x I domain in the absence of any ligand. By titrating at potential lead compound and acquiring HSQC spectra, residues affected by ligand binding can be identified. Furthermore, the affinity of the protein to such compound can be calculated using HSQC data.

Leukocyte integrins have increasingly become targets for therapeutic intervention in disease. Lifitegrast, a small molecule antagonist of the $\alpha_L\beta2$ integrin was recently FDA approved for the treatment of dry eye disease. (Abidi *et al.*, 2016) Natalizumab is an antibody targeted to α_4 integrins approved for treating the symptoms of multiple sclerosis

(Hutchinson, 2007). Vedolizumab, an antibody targeted to the $\alpha_4\beta_7$ integrin has been approved for the treatment of ulcerative colitis and chron's disease (Singh *et al.*, 2016). These therapeutics highlight the promise of integrin-based therapeutics- local anti-inflammatory effects without the global immune suppression typically associated with steroid medications. This would enable for the targeted treatment of disease while simultaneously allowing the patient immune system to combat infections. The α_x integrin is expressed on dendritic cells, monocytes, and macrophages, but not T cells. Hence, drugs targeting the $\alpha_x\beta2$ integrin can have a therapeutic effect, while maintaining the ability of T cells to respond to an infection.

Several statin drugs, which are typically used to inhibit the production of cholesterol, have been reported to selectively bind and inhibit integrin proteins (Weitz-Schmidt *et al.*, 2001; Jensen *et al.*, 2016). A crystal structure has been published, in which Simvastatin binds to the αI domain of the $\alpha_M\beta2$ integrin. An image of this crystal structure is presented in Figure 14. The hydroxyl acid moiety of simvastatin binds to the Mg^{2+}, resembling the interactions of asp242 and glu244 with Mg^{2+} in the MIDAS. This binding competitively inhibits integrin interaction with extracellular ligands. In an *in vitro* experiment, simvastatin inhibited adhesion of primary human monocytes to iC3b. (Jensen *et al.*, 2016) Hence, analogs of statin drugs optimized for selective binding to integrins could be promising anti-inflammatory medications.

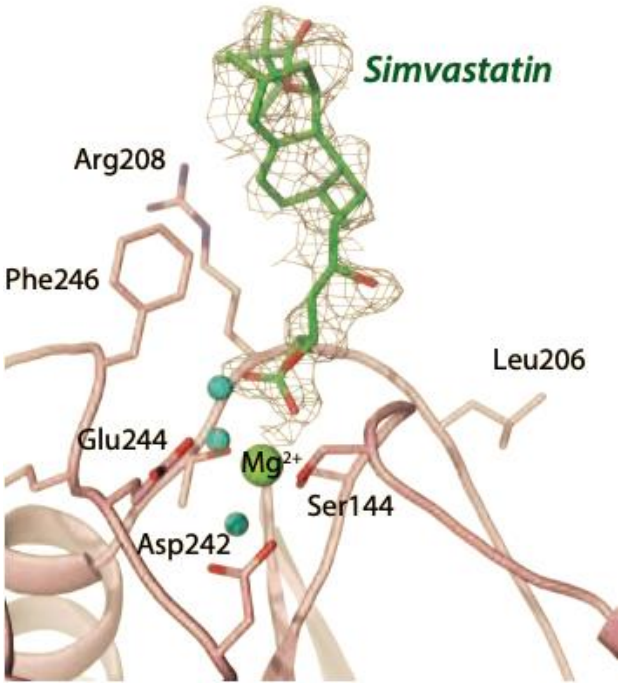

Figure 12: Crystal Structure of α_M I Domain Complexed with Simvastatin

Simvastatin binding at the Metal Ion Adhesion Site of the α_M I domain. The drug binds to the Magnesium Ion through its hydroxyl acid moiety. Contacts of Ser144, Glu244 and Asp 242 to Mg^{2+} are also shown. Figure adapted from Jensen *et al.*, 2016.

Future experiments could involve NMR spectroscopy of the α_x I Domain upon titration with statin drugs, such as simvastatin. Such experiments would probe analogous binding of these drugs to the MIDAS region. Exploiting the residues specifically found in the α_x I Domain and not in other integrin I domains could lead to development of inhibitor drugs selective to the protein.

REFERENCES

Abidi, A., Shukla, P., and Ahmad, A. (2016). Lifitegrast: A novel drug for treatment of dry eye disease. Journal of Pharmacology and Pharmacotherapeutics *7*, 194-198.

Aplin, A.E., Howe, A., Alahari, S.K., Juliano, R.L., and Hill, C. (1998). Signal Transduction and Signal Modulation by Cell Adhesion Receptors : The role of integrins , cadherins, immunoglobulin-cell adhesion molecules, and selectins. Pharmacology Reviews *50*, 197–252.

Burridge, K., and Chrzanowska-wodnicka, M. (1996). Focal adhesions, contractility, and Signaling. Cell Developmental Biology *12*, 463–519.

Cavanagh, J., Palmer, A. G., Skelton, N. J., and Fairbrother, W. J. (2007). Heteronuclear NMR experiments In J. Cavanagh, Protein NMR spectroscopy: principles and practice. Academic Press. 535-660

Chen, X., Xie, C., Nishida, N., Li, Z., Walz, T., and Springer, T.A. (2010). Requirement of open headpiece conformation for activation of leukocyte integrin α X β 2. Proceedings of the National Academy of Sciences *107*, 14727–14732.

Curtis, J.L., and Morrison, V.L. (2017). β 2 integrins as regulators of dendritic cell, monocyte, and macrophage function. Frontiers Immunology *8*, 1–11.

Frick, C., Odermatt, A., Zen, K., Mandell, K.J., Edens, H., Portmann, R., Mazzucchelli, L., Jaye, D.L., and Parkos, C.A. (2005). Molecular immunology interaction of ICAM-1 with b 2-integrin CD11c / CD18 : Characterization of a peptide ligand that mimics a putative binding site on domain D4 of ICAM-1. European Journal of Immunology *35*, 3610–3621.

Hutchinson, M. (2007). Natalizumab : A new treatment for relapsing remitting multiple sclerosis. Therapeutics and Clinical Risk Management *3*, 259–268.

Hynes, R.O. (2002). Integrins : bidirectional, allosteric signaling machines in their roles as major adhesion receptors, integrins. Cell *110*, 673–687.

Jawhara, S., Pluskota, E., Cao, W., Plow, E.F., and Soloviev, D.A. (2017). Distinct Effects of Integrins α X β 2and α M β 2 on leukocyte subpopulations during inflammation and antimicrobial responses. Infections and Immunity *85*, 1–17.

Jensen, M.R., Bijac, G., Zhang, X., Lausten, A.K., Koldson, H., Skeby, K.K., Schiott, B., Andersen, G.R., and Vorup-Jensen, T. (2016). Simvastatin antagonism of complement receptor 3. Journal of Biological Chemistry *291*, 16963–16976.

Johnson, B. (2004) Using NMRView to visualize and analyze the NMR spectra of macromolecules In A. K. Dowling Protein NMR techniques. Humana Press. 313–352.

Kallen, J., Welzenbach, K., Ramage, P., Geyl, D., Kriwacki, R., Legge, G., Cottens, S., and Hommel, U. (1999). Structural basis for LFA-1 inhibition upon lovastatin binding to the CD11a I-Domain. Journal of Molecular Biology *292*, 1–9.

Kiema, T., Lad, Y., Jiang, P., Oxley, C.L., Baldassarre, M., Wegener, K.L., Campbell, I.D., Yla, J., and Calderwood, D.A. (2006). The molecular basis of filamin binding to integrins and competition with talin. Molecular Cell *21*, 337–347.

Kim, M., Carman, C. V, and Springer, T.A. (2003). Bidirectional transmembrane signaling by cytoplasmic domain separation in integrins. Science *301*, 1720–1726.

Lee, J., Rieu, P., Arnaout, M.A., and Liddington, R. (1995). Crystal structure of the A domain from the a subunit of integrin CR3 (CD11b / CD18). Cell *80*, 631–638.

Lee, W., Tonelli, M., and Markley, J.L. (2015). Structural bioinformatics NMRFAM-SPARKY : enhanced software for biomolecular NMR spectroscopy. Bioinformatics *31*, 1325–1327.

Ley, K., Rivera-Nieves, J., Sandborn, W.J., and Shattil, S. (2016). Integrin-based therapeutics: biological basis, clinical use and new drugs. National Reviews Drug Discovery *15*, 173–183.

Manandhar, P., Abousaway, O., Le, T., and Sen, M. (2017). Role of structural dynamics in leukocyte integrins function : interplay between the shape-shifting mechanism and allostery. International Journal of Cell Science and Molecular Biology *3*, 1–4.

Muller, W.A. (2013). Getting leukocytes to the site of inflammation. Veterinary Pathology *50*, 7–22.

Nishida, N., Xie, C., and Springer, T.A. (2006). Activation of leukocyte β 2 integrins by conversion from bent to extended conformations. Immunity *25*, 583–594.

Parsons, J.T. (2003). Focal adhesion kinase: the first ten years. Journal of Cell Science *116*, 1409–1416.

Schlaepfer, D.D., Hankst, S.K., Hunter, T., and Geer, P. Van Der (1994). lntegrin-mediated signal transduction linked to Ras pathway by GRB2 binding to focal adhesion kinase. Nature *372*, 786–791.

Sen, M., and Springer, T.A. (2016). Leukocyte integrin α L β 2 headpiece structures : The α I domain, the pocket for the internal ligand, and concerted movements of its loops. Proceedings of the National Academy of Sciences *113*, 2940–2945.

Sen, M., Yuki, K., and Springer, T.A. (2013). An internal ligand-bound, metastable state of a leukocyte integrin,aXb2. Journal of Cell Biology *203*, 629–642.

Shimaoka, M., Xiao, T., Liu, J., Yang, Y., Dong, Y., Jun, C., Mccormack, A., Zhang, R., Joachimiak, A., Takagi, J., et al. (2003). Structures of the α L I domain and its complex with ICAM-1 reveal a shape-shifting pathway for integrin regulation. Cell *112*, 99–111.

Singh, H., Grewal, N., Arora, E., Kumar, H., and Kakkar, A. K. (2016). Vedolizumab: a novel anti-integrin drug for treatment of inflammatory bowel disease. Journal of Natural Science, Biology, and Medicine *7*, 4-9.

Stewart, M., Thiel, M., and Hogg, N. (1995). Leukocyte integrins. Current Opinion Cell Biology *7*, 690–696.

Takagi, J., and Springer, T.A. (2002). Integrin activation and structural rearrangement. Immunology Reviews *186*, 141–163.

Vorup-Jensen, T., Ostermeier, C., Shimaoka, M., Hommel, U., and Springer, T.A. (2003). Structure and allosteric regulation of the α X β 2integrin I domain. Proceedings of the National Academy of Sciences *100*, 1873–1878.

Weitz-Schmidt, G., Welzenbach, K., Brinkmann, V., Kamata, T., Kallen, J., Bruns, C., Cottens, S., Takada, Y., and Hommel, U. (2001). Statins selectively inhibit leukocyte function antigen-1 by binding to a novel regulatory integrin site. Nature *7*, 687–692.

Xie, C., Zhu, J., Chen, X., Mi, L., Nishida, N., and Springer, T.A. (2009). Structure of an integrin with an α I domain , complement receptor type 4. EMBO Journal *29*, 666–679.

Xu, S., Wang, J., Wang, J., and Springer, T.A. (2017). Distinct recognition of complement iC3b by integrins. Proceedings of the National Academy of Sciences *114*, 3403–3408.

APPENDIX

To prepare 1L minimal media for $^{13}C/^{15}N$ labelling:

200mL 5X M9 Solution
2mL 1M $MgSO_4$
100µL 1M $CaCl_2$
10mL 100X Vitamin Solution
20mL $^{15}NH_4(Cl)_2$
20mL 20% D-Glucose (^{13}C-labelled)
4mL Solution Q
Antibiotics
Autoclaved H_2O to 1L
Antibiotics

To prepare 1L minimal media for $^{2}D/^{13}C/^{15}N$ labelling:

100mL 10X M9 Solution (prepared with D_2O)
2mL 1M $MgSO_4$ (prepared with D_2O)
100µL 1M $CaCl_2$
10mL 100X Vitamin Solution
20mL $^{15}NH_4(Cl)_2$
20mL 20% D-Glucose (^{13}C-labelled)
4mL Solution Q
Antibiotics
Filter sterilized D_2O to 1L
Antibiotics

Table AI: Chemical Shift Table of α_x I Domain

Residue	N	HN	Ca	Cb	C'
Q131	119.244	7.961	34.542	58.328	166.841
D132	127.996	9.009	36.338	48.121	167.847
I133	122.245	8.274	28.884	51.808	168.764
L136	127.052	9.549	36.054	44.366	
D138	125.164	8.387	32.752		170.134
G139	115.518	7.858	42.966		
S140	115.653	9.463	30.674		169.383
G141	104.364	8.546	43.216		168.04
I143	126.249	7.582	26.775		169.843

Table AI Continued

S144	123.685	8.508	24.197	31.937	168.629
S145	116.981	9.021	27.438	26.596	172.564
R146	122.175	8.353	30.271	59.583	172.572
N147	119.131	7.514	34.102	52.043	170.467
F148	123.732	9.021	26.588	50.558	171.433
A149	120.268	7.676	33.635	72.097	175.027
T150	118.343	8.088	22.687	21.5	171.657
M151	124.862	8.527	29.214	57.26	171.897
M152	117.646	8.174	33.64	61.504	173.765
N153	119.777	8.252	33.53	51.822	172.208
F154	123.928	7.759	28.576	51.311	169.595
R156	121.933	8.766	32.254		167.182
A157	109.725	8.17	33.072		168.968
I159	118.608	8.087	23.355		173.114
S160	111.514	7.838	28.185	25.54	168.926
Q161	118.434	7.79	33.2	60.47	169.313
F162	118.189	7.745	31.637	47.3	169.498
Q163	120.425	9.136	33.499	58.576	170.242
R164	122.71	8.747	34.366	58.805	170.343
S166	120.235	8.483	25.409	26.923	171.437
S167			25.106	19.914	167.261
Q168	129.577	8.943	33.275	55.709	168.762
S170	108.884	8.02	33.408	24.901	165.955
L171	124.964	6.694	35.435	43.306	168
M172	128.514	9.198	35.622	51.925	166.73
Q173	128.931	9.465	36.515	56.924	167.902
F174	124.301	9.506	34.379	43.656	165.825
S175	118.19	8.788	31.208	26.802	170.141
N176	119.379	8.499	35.423	51.219	166.575
K177	119.356	7.208	35.606	54.386	167.652
F178	115.73	8.256	32.901	48.295	169.377
Q179	123.8	9	34.168	57.978	168.379
T180	127.092	9.221	26.164	21.884	168.657
H181	129.563	8.58	29.864	60.39	170.401
F182	108.155	6.978	33.056	49.351	169.823
T183	116.185	9.38	29.164	18.108	168.99

Table AI Continued

F184	119.794	8.544	27.563	50.588	172.5
E185	118.116	8.135	30.318	60.219	172.858
E186	118.234	7.852	30.055	59.27	173.886
F187	121.21	8.631	26.879	48.664	171.882
R188	119.635	9.011	30.163	59.679	172.629
R189	114.167	7.849	32.335	58.602	171.137
S190	113.24	7.035	30.518	25.248	170.333
N192	116.384	8.033	38.435	51.079	167.371
L194	115.021	7.958	31.961	49.947	175.092
S195	115.646	7.984	27.969	25.994	171.104
L196	122.009	7.449	32.658	48.533	172.781
L197	114.995	7.141	33.58	48.635	171.851
A198	120.896	7.29	34.819	70.832	172.314
S199	110.264	7.542	31.804	25.818	167.735
V200	122.444	7.062	26.076	58.194	168.701
H201	126.384	8.296	35.521	58.551	169.046
Q202	127.541	8.624	33.386	62.209	171.968
L203	128.812	9.484	36.515	45.62	175.157
Q204	107.929	7.357	31.149	62.918	168.763
G205	104.17	7.948	45.056		169.435
F206	121.528	7.083	31.972	50.922	166.109
T207	111.151	7.753	27.584	19.235	169.632
Y208	128.567	8.871	35.842	55.202	171.37
T209	111.749	7.531	23.542	20.699	170.968
A210	120.328	7.678	33.635	72.079	175.027
T211	121.032	10.448	21.321	22.074	171.181
A212	123.433	8.265	33.229	70.018	172.962
I213	117.778	7.862	23.003	51.874	171.402
Q214	120.587	8.215	29.259	60.946	171.57
N215	116.584	7.808	32.63	50.259	171.998
V216	120.6	8.02	22.136	58.244	171.023
V217	116.336	8.139	22.407	60.307	171.603
H218	112.824	8.197	31.406	57.844	170.874
R219	113.982	7.841	32.335	58.602	169.668
L220	114.838	7.036	30.452	49.086	172.352
F221	110.061	7.219	30.386	51.516	168.369

Table AI Continued

H222	121.564	7.679	30.997	56.533	171.88
A223	131.596	8.623	33.744	70.933	175.921
S224	117.99	10.748	27.54		170.275
Y225	123.913	8.292	31.222	51.612	170.281
G226	104.828	8.207	43.817		168.839
A227	123.907	7.208	36.577	70.334	123.907
R228	126.215	0.086	33.314	58.496	171.722
R229	125.543	8.607	29.902	59.178	171.816
D230	115.111	8.636	35.088		169.842
A231	121.359	6.89	37.167	69.717	171.822
T232	120.127	8.633	25.156	23.948	
L235	129.089	9.593	36.634		167.839
I236	127.092	9.342	28.52		167.902
V237	127.671	8.97	28.105		
G241	111.161	8.629	44.746		
K243	124.228	9.601	31.579	57.882	171.791
E244	127.558	8.883	32.703	56.585	169.489
G245	112.857	8.66	43.717		166.493
D246	120.18	6.751	36.344	46.669	171.246
S247	122.648	8.424	29.209	25.928	168.337
L248	122.575	7.97	35.756	45.909	169.501
D249	121.068	9.043	37.33	45.353	171.915
Y250	122.101	8.454	26.253	53.086	173.093
K251	117.322	8.869	30.908	58.609	170.397
D252	115.418	7.378	33.171	46.541	171.225
V253	112.353	7.523	27.053	54.978	169.49
I254	123.344	8.739	26.604	57.234	169.474
M256	115.572	7.561	30.813	57.866	173.017
A257	123.719	7.754	34.344	72.015	173.154
D258	118.397	8.586	31.903	49.777	174.933
A259	124.015	8.237	34.422	71.817	173.142
A260	117.476	7.191	37.347	70.419	171.369
G261	106.859	7.751	43.283		168.681
I262	119.046	7.479	28.139	51.095	169.723

Table AI Continued

I263					
R264	124.558	8.898	34.931	58.623	169.954
Y265	121.649	9.434	32.242	47.832	168.809
A266	123.054	8.727	38.753	66.861	168.378
I267	124.02	9.359	29.126	51.308	168.41
G268	112.729	8.536	44.013		166.366
V269	125.005	8.673	28.95	55.736	171.159
G270	109.924	7.928	44.51		170.472
L271	119.9	8.639	31.574	47.324	173.612
A272	121.259	9.065	37.364	71.02	173.268
F273	110.808	7.139	31.657	51.125	169.752
Q274	118.034	7.474	31.654	60.146	170.767
N275	116.058	8.019	36.551	49.432	170.213
N277	117.463	8.59	33.734	51.722	171.499
S278	115.821	7.991	28.613	24.733	170.235
W279	122.166	7.642	30.73	61.096	171.914
K280	120.213	7.875	29.742	57.509	171.286
E281	118.04	7.505	29.599	59.779	172.052
L282	112.863	6.812	32.157	49.771	172.744
N283	117.033	7.76	33.558	51.19	171.43
D284	118.541	8.153	32.645	49.152	172.929
I285	119.113	6.917	25.094	49.44	170.197
A286	119.477	7.558	36.836	68.07	172.616
S287	119.08	8.357	28.278	27.35	165.66
K288	118.338	8.236	35.505	57.653	170.187
S291	115.646	7.984	27.969	25.994	171.658
E292	113.397	7.012	33.257	59.295	170.235
H293	114.302	7.76	32.777	58.201	165.863
I294	115.741	6.692	29.607	47.387	169.364
F295	122.511	8.946	32.55	46.808	167.646
K296	122.754	8.64	33.949	57.268	169.83
V297	120.532	8.607	29.458	55.241	171.012
E298	125.687	9.325	29.332	59.36	169.397
D299	110.25	7.1	36.645	47.281	169.969
F300	117.084	8.691	26.463	50.817	172.49

Table AI Continued

D301	119.774	8.373	32.156	49.227	169.891
A302	119.765	7.55	37.197	70.185	173.389
L303	121.34	7.476	31.249	49.815	172.449
K304	113.957	8.026	31.017	58.44	172.237
D305	119.052	7.481	32.898	48.676	172.2
I306	110.596	7.711	28.221	51.156	17.656
Q307	120.818	7.231	28.885	60.483	171.314
N308	116.858	8.694	33.404	51.817	171.582
Q309	120.66	8.165	30.269	60.267	172.854
L310	119.418	8.167	30.988	48.316	171.488
K311	117.493	7.587	28.915	58.091	171.612
E312	116.35	8.152	29.855	60.307	174.328
K313	118.663	7.98	29.884	57.726	173.65
I314	119.82	7.851	24.368	51.566	173.288
F315	116.787	7.969	29.206	59.166	171.884
A316	121.594	7.881	34.329	71.695	175.184
E318	121.805	8.477	32.851	58.952	171.27
G319	110.113	8.481	43.982		168.273

----------DATA NOT FINALIZED-REQUIRES REPROCESSING----------